JGP Journal of General Physiology

RESEARCH ARTICLE

# Physiological CRAC channel activation and pore properties require STIM1 binding to all six Orai1 subunits

Michelle Yen and Richard S. Lewis

**The binding of STIM1 to Orai1 controls the opening of store-operated CRAC channels as well as their extremely high $Ca^{2+}$ selectivity. Although STIM1 dimers are known to bind directly to the cytosolic C termini of the six Orai1 subunits (SUs) that form the channel hexamer, the dependence of channel activation and selectivity on the number of occupied binding sites is not well understood. Here we address these questions using dimeric and hexameric Orai1 concatemers in which L273D mutations were introduced to inhibit STIM1 binding to specific Orai1 SUs. By measuring FRET between fluorescently labeled STIM1 and Orai1, we find that homomeric L273D mutant channels fail to bind STIM1 appreciably; however, the L273D SU does bind STIM1 and contribute to channel activation when located adjacent to a WT SU. These results suggest that STIM1 dimers can interact with pairs of neighboring Orai1 SUs. Surprisingly, a single L273D mutation within the Orai1 hexamer reduces channel open probability by ∼90%, triples the size of the single-channel current, weakens the $Ca^{2+}$ binding affinity of the selectivity filter, and lowers the selectivity for $Na^+$ over $Cs^+$ in the absence of divalent cations. These findings reveal a surprisingly strong functional coupling between STIM1 binding and CRAC channel gating and pore properties. We conclude that under physiological conditions, all six Orai1 SUs of the native CRAC channel bind STIM1 to effectively open the pore and generate the signature properties of extremely low conductance and high ion selectivity.**

## Introduction

Store-operated calcium channels serve many physiological functions, ranging from immune cell activation and sustained muscle activity to migration, secretion, and gene expression in a wide variety of cells (Prakriya and Lewis, 2015). They are activated by receptors that generate inositol 1,4,5-trisphosphate; the release of $Ca^{2+}$ through inositol 1,4,5-trisphosphate receptors in the ER (the calcium "store") is sensed by STIM1, a dimeric ER protein that subsequently oligomerizes and accumulates at ER-plasma membrane (ER-PM) junctions (Liou et al., 2005; Zhang et al., 2005; Wu et al., 2006; Luik et al., 2008). At these sites, clusters of STIM1 trap and activate Orai1, the pore-forming subunit (SU) of the $Ca^{2+}$ release-activated $Ca^{2+}$ (CRAC) channel, to trigger $Ca^{2+}$ entry across the plasma membrane (Luik et al., 2006; Prakriya et al., 2006). Two of the characteristic features of the CRAC channel are its extremely high $Ca^{2+}$ selectivity, which ensures that only $Ca^{2+}$ enters the cell under physiological conditions, and its extremely low $Ca^{2+}$ conductance of 20–40 femtosiemens estimated from noise analysis (Zweifach and Lewis, 1993; Hoth, 1995; Prakriya and Lewis, 2006). These and other signature properties are reproduced by artificially constructed hexameric concatemers of Orai1, providing functional support for crystallographic evidence that the CRAC channel comprises a hexamer of Orai1 SUs (Hou et al., 2012; Cai et al., 2016; Yen et al., 2016).

Given the unusual way in which CRAC channels are regulated, the molecular details of the activation process are of particular interest. STIM1 binds directly to the C termini of Orai1 to open the channel via an ∼100–amino acid cytosolic domain variously termed the CRAC activation domain (CAD, aa 342–448; Park et al., 2009), STIM-Orai activation region (SOAR, aa 344–442; Yuan et al., 2009), or Ccb9 (aa 339–444; Kawasaki et al., 2009). Under resting conditions, the CAD is masked by interactions with the coiled-coil 1 domain that attaches it to the ER membrane; ER $Ca^{2+}$ depletion initiates a series of conformational changes in STIM1 that propagate from the ER lumen to the cytosol to release coiled-coil 1 and allow CAD to bind and activate Orai1 (Stathopulos et al., 2008; Zhou et al., 2013; Ma et al., 2015; Hirve et al., 2018). Published work supports two differing views of how STIM1 may engage Orai1. An NMR solution structure of a complex of purified STIM1 and Orai1 fragments depicts a

Department of Molecular and Cellular Physiology, Stanford University School of Medicine, Stanford, CA.

Correspondence to Richard S. Lewis: rslewis@stanford.edu.

STIM1 dimer bound to two Orai1 C termini ("dimeric binding"; Stathopulos et al., 2013). In contrast, experiments with dimeric SOAR concatemers containing a nonbinding mutant SU support the idea that only one SU of each STIM1 dimer need bind to each Orai1 C terminus to activate the channel ("monomeric binding"; Zhou et al., 2015).

Given the rather large number of STIM1 binding sites on the Orai1 hexamer, a central question is how CRAC channel activation depends on the extent of STIM1 binding. One experimental approach to this question is to introduce mutations into the Orai1 C terminus to reduce the number of bound STIM1s. Numerous Orai1 mutations are known to weaken binding to STIM1, but the L273D mutation is among the most potent inhibitors and is widely considered to completely block binding (Cai et al., 2016; Zhou et al., 2016). Homomultimers of Orai1(L273D) fail to bind STIM1 as assayed by recruitment of CAD/SOAR fragments to the plasma membrane (Li et al., 2011) or coclustering with STIM1 in store-depleted cells (Zhou et al., 2016), resulting in a complete lack of channel activity (Li et al., 2011; Zhou et al., 2016; Vaeth et al., 2017). In tetrameric Orai1 concatemers, activation appeared graded with the number of L273D mutations introduced (Li et al., 2011), but a clear interpretation of this result was complicated by subsequent structural and functional studies indicating a hexameric channel stoichiometry (Hou et al., 2012; Cai et al., 2016; Yen et al., 2016). In another study, Hoover and Lewis (2011) showed that in cells expressing similar levels of STIM1, CRAC current increased with Orai1 expression level until the STIM1:Orai1 ratio fell below ∼2, at which point further increases in Orai1 caused an abrupt drop in current. These studies revealed a highly nonlinear dependence of channel activity on the STIM1:Orai1 ratio, although the number of bound STIM1s per channel was not assessed.

An unusual feature of the CRAC channel is that STIM1 binding not only opens the channel, but also confers its characteristically high $Ca^{2+}$ selectivity (Scrimgeour et al., 2009; McNally et al., 2012). Constitutively active Orai1 mutant V102C channels are nonselective unless STIM1 is coexpressed, and partially active channels made from Orai1-SOAR chimeras or by expressing Orai1 in excess of STIM1 display reduced selectivity, which can be rescued by addition of STIM1 (McNally et al., 2012). Although these studies clearly demonstrate that STIM1 binding controls CRAC channel opening as well as its characteristic ion selectivity, the relation between the number of occupied binding sites and ion selectivity is unknown.

To gain a better understanding of how STIM:Orai binding stoichiometry determines CRAC channel activity and selectivity, we introduced STIM1-binding mutations into dimeric and hexameric Orai1 concatemers. Concatemers allowed us to control the number and placement of STIM1-binding mutations and to measure their impact on binding, activation, and ion permeation. We find that STIM1 can bind to an L273D Orai1 SU when it is adjacent to a WT SU, suggesting that STIM1 can interact with pairs of Orai1 C termini. The effects of mutating single Orai1 SUs indicate that all six of the STIM1 binding sites on Orai1 must be occupied to activate the channel significantly and to confer its signature pore properties of high ion selectivity and extremely low conductance.

## Materials and methods

### DNA constructs

Orai1 hexameric concatemers comprised six Orai1 SUs concatenated with a 24-aa linker sequence containing a SU-specific restriction enzyme site, Tobacco Etch Virus–protease recognition site, myc epitope tag, and Gly-Ser stretch, and labeled at the C terminus with EGFP as previously described (Yen et al., 2016). To generate mutant hexamers, the mutations were first introduced into TOPO vectors (Life Technologies) carrying individual SUs. L273D mutants were generated by site-directed mutagenesis on individual SUs, the ΔCT deletion mutant was constructed by using primers flanking the region to be deleted (aa Δ266–301), and the polymutant (L273D, L276D, R281A, D284A, L286S, D287A, R289A, D291A) was created by sequential rounds of mutagenesis. Mutant SUs were digested from TOPO vectors and ligated into hexamer plasmids to replace a WT SU with a mutant.

To construct Orai1 dimers, the first two SUs of the Orai1 hexamer were excised using XhoI and EcoRI (Fermentas) and ligated into either ECFP-C1 (Clontech) to generate an N-terminally fused CFP-2xOrai1 or into EGFP-N1 (Clontech) to generate C-terminally fused 2xOrai1-GFP. To generate mutant dimers, individual Orai1 SUs were subcloned into pCR-BLUNT II-TOPO vectors (Thermo Fisher Scientific) and mutated via site-directed mutagenesis before digestion and ligation into the dimer backbone. Additionally, a stop codon was introduced after the second Orai1 SU for CFP-2xOrai1 plasmids.

#### *Other plasmids*

We have previously described the construction of mCherry-STIM1 (Wu et al., 2006), YFP-CAD (Park et al., 2009), and STIM1-YFP (Rana et al., 2015). Orai1-GFP was a gift from T. Xu (University of Chinese Academy of Sciences; Li et al., 2007), and YFP-S-S was a gift from D. Gill (Penn State College of Medicine; Zhou et al., 2015). All plasmids were verified by sequencing (Sequetech Corp. or MCLAB).

### Cell culture and transfection

Human embryonic kidney (HEK)293-H cells (ATCC) were passaged adherently in Dulbecco's Modified Eagle's medium media containing 10% FBS, 2 mM L-alanyl-glutamine, and 100 U/ml penicillin/streptomycin and cultured at 37°C in 5% $CO_2$. Lipofectamine-mediated transfections (Thermo Fisher Scientific) were performed on 6-cm dishes using a total of 0.8 µg DNA, and a 10:1 mass ratio of mCherry-STIM1 to Orai1 hexamer–GFP. Prior to experiments, cells were maintained for 2 d after transfection at 30°C for Orai1 hexamer variants (to maximize surface expression) or at 37°C for Orai1 dimers. Cell culture reagents were purchased from Gemini Biosciences.

### Solutions

2 mM $Ca^{2+}$ Ringer's solution contained (in mM) 155 NaCl, 4.5 KCl, 2 $CaCl_2$, 1 $MgCl_2$, 10 D-glucose, and 5 HEPES (pH 7.4 with NaOH). 20 mM $Ca^{2+}$ Ringer's was similar to 2 mM $Ca^{2+}$ Ringer's but contained 130 mM NaCl and 20 mM $CaCl_2$. For $Na^+$-free 2 mM $Ca^{2+}$ Ringer's, $Na^+$ was replaced with equimolar NMDG-Cl (pH 7.4 with HCl). Divalent-free (DVF) Ringer's contained (in mM) 150

NaCl, 0.5 EDTA, 10 TEA-Cl, and 20 HEPES (pH 7.4 with NaOH). DVF Ringer's with μM free $Ca^{2+}$ contained (in mM) 122 NaCl, 10 HEDTA, 1 EDTA, 10 TEA-Cl, and 10 HEPES (pH 7.4 with NaOH), and MaxChelator was used to calculate the total $CaCl_2$ added to achieve the desired free $Ca^{2+}$ concentration. The resulting $Ca^{2+}$ concentrations were measured using a calibrated $Ca^{2+}$-sensitive electrode (Thermo Orion). All DVF solutions contained a total $[Na^+]$ of 160 mM, and an osmolarity of 315 ± 3 mOsm (mean ± SEM), as determined with a Fiske freezing point depression microosmometer (Advanced Instruments). Recording pipette solution contained (in mM) 150 Cs aspartate, 8 $MgCl_2$, 10 EGTA, and 10 HEPES (pH 7.2 with CsOH). All chemical reagents were purchased from Sigma.

### FRET microscopy

Prior to imaging, cells were trypsinized into suspension and plated for 30–60 min at 37°C. Cells expressing full-length STIM1 were store-depleted with 1 μM thapsigargin (EMD Millipore) in 0 mM $Ca^{2+}$ Ringer's for 10 min before imaging, whereas cells expressing soluble CAD or SOAR constructs were imaged in 2 mM $Ca^{2+}$ Ringer's. Experiments were performed on a Zeiss Axiovert 200M microscope (Zeiss) controlled by μManager software, using a Polychrome II xenon light source for illumination (TILL Photonics) and 40× Fluar oil-immersion objective (NA 1.3). The filter sets used were the following: 436 ± 10 excitation, 455 DCXR dichroic, and 485 ± 20 nm emission for CFP; ET500 ± 10 excitation, 515 DCXR dichroic, and 535 ± 15 nm emission for YFP; and 436 ± 10 excitation, 455 DCXR dichroic, and 535 ± 15 nm emission for FRET. All filters were purchased from Chroma Technology Corp. Images were collected with an ORCA-ER CCD camera with 1 × 1 binning or an ORCA FLASH sCMOS camera using 2 × 2 binning (Hamamatsu). FRET was quantified using the E-FRET method (Zal and Gascoigne, 2004). FRET analysis was restricted to cells with molar STIM1:Orai1 ratios > 2:1 to ensure that STIM1 abundance was not limiting. Raw images were background subtracted, and average E-FRET calculated for an ∼0.65-μm (2 pixel width) band around the cell periphery using the following formulae (Zal and Gascoigne, 2004):

$$E\text{-}FRET = F_c/(F_c + GI_{DD}), \quad (1)$$

where $F_c$ is the sensitized emission, G is an instrument-dependent factor, and $I_{DD}$ is the background-corrected CFP image, and

$$F_c = I_{DA} - a(I_{AA} - cI_{DD}) - d(I_{DD} - bI_{AA}), \quad (2)$$

where $I_{DA}$ and $I_{AA}$ are the background-corrected images for FRET and YFP, respectively. Cells singly expressing CFP or YFP were used to determine bleedthrough coefficients ($a$ = 0.064, $b$ = 0.016, $c$ = 0, $d$ = 0.493), and G (3.58) was determined by measuring donor recovery after acceptor photobleaching using cells expressing a YFP-CFP calibrator construct, CFP-receptor protein-tyrosine phosphatase (RPTP)-SpD2-YFP2.1 (Blanchetot et al., 2002). For each FRET acceptor (STIM1-YFP, YFP-CAD, or YFP-S-S), FRET with all five Orai1 dimer variants was measured concurrently. Transfections of each FRET pair were performed at least twice, and data from multiple experiments were pooled together. Transfections for the YFP-CAD and YFP-S-S FRET series were performed on the same parental batch of HEK293 cells. All statistical tests were performed using Prism (GraphPad Software).

### Diamide cross-linking of Orai1 tandem dimers

HEK293-H cells were transfected with CFP-2xOrai1 or Orai1(L-273C)-GFP (positive control) 2 d before cross-linking. Immediately before cross-linking, cells were trypsinized into suspension and washed twice with PBS before resuspension at 1.5–2 × $10^6$ cells/ml in 2 mM $Ca^{2+}$ Ringer's. Cross-linking was performed with 0.25 mM diamide (Sigma) in 2 mM $Ca^{2+}$ Ringer's for 10 min at 22–24°C. After cross-linking, cells were washed with PBS and lysed in radioimmunoprecipitation assay buffer containing 10 mM N-ethylmaleimide (EMD MIliipore) to cap unreacted sulfhydryls. Lysates were sheared five times with a 27-gauge needle, centrifuged for 10 min at 14,000 rpm at 4°C to pellet debris, and treated with Peptide N-Glycosidase F (New England Biolabs) for 1.5 h at 37°C to deglycosylate Orai1. Subsequently, samples were mixed with 4× lithium dodecyl sulfate sample buffer (Life Technologies) ± 100 mM dithiothreitol and resolved on 4–12% Bis-Tris polyacrylamide gels (Thermo Fisher Scientific). Proteins were transferred to polyvinylidene fluoride membranes (GE Healthcare Life Science) and stained with polyclonal anti-Orai1 antibody (1:2,500; Sigma) followed by anti–rabbit IR-680 secondary (1:10,000; LI-COR), and visualized using the LiCor Odyssey system (LI-COR). The diamide cross-linking experiment was performed twice (two independent transfections) with similar results.

### Electrophysiology

A previous study suggests that a protein expression ratio of ≥ 2 STIM1:Orai1 is required for maximal channel activation (Hoover and Lewis, 2011). To compare current amplitudes across hexamer variants, we ensured that STIM1 abundance was not limiting by selecting cells having a mCherry:GFP fluorescence ratio corresponding to > 5:1 STIM1:Orai1, as determined by a mCherry-GFP calibrator construct (Hoover and Lewis, 2011). mCherry and GFP fluorescence were evaluated by widefield imaging at the cell equator using a Zeiss 200M Axiovert microscope with a 40× Fluar oil-immersion objective (NA 1.3). A Polychrome II monochromator with xenon lamp (TILL Photonics) was used for excitation, with a GFP filter set (488 ± 10 excitation, 515 dichroic, 535 ± 15 nm emission), an mCherry filter set (535 ± 20 excitation, 565 dichroic, 660 ± 25 nm emission), and an ORCA-ER CCD camera. All filters were from Chroma Technology Corp. The data for each Orai1 variant were collected from three to five independent transfections. Electrophysiology experiments comparing Orai1 variants were performed concurrently when possible, including the data shown in Figs. 1, 3, and 5.

Patch-clamp recording was performed at 21–24°C using recording electrodes pulled from borosilicate glass capillary tubes with tip resistances of 2–5 MΩ, an Axopatch 200 or 200B amplifier (Axon Instruments/Molecular Devices), an InstruTECH ITC-16 interface (HEKA Instruments) and a Mac Mini computer (Apple). After seal formation and break-in, CRAC current ($I_{CRAC}$) was induced through passive ER store depletion by 10 mM EGTA in the patch pipette. Voltage commands (100-ms step to −100 mV followed by a 100-ms ramp to +100 mV) were delivered to the cell every 5 s from a holding potential of +30 mV to monitor

development of CRAC current. After $I_{CRAC}$ reached a maximum, current amplitude was determined by the peak current during steps to −100 mV. Whole-cell currents were leak subtracted using 10–100 µM $LaCl_3$ in 2 or 20 mM $Ca^{2+}$ Ringer's. Solutions were locally perfused with a valve manifold system attached to an eight-channel perfusion pencil with a 360-µm diameter tip (AutoMate Scientific) that was positioned near the cell. To measure the speed of solution exchange, solutions of varying ionic strength were perfused from the pencil tip onto a glass recording pipette under current clamp while monitoring changes in voltage. The system achieved a local exchange time of < 2 s. Voltage values were corrected for liquid junction potentials between the Cs aspartate in the recording pipette and 2 mM $Ca^{2+}$ Ringer's in the bath (−13 mV), and between NMDG-containing perfusion solutions and the bath (+3.5 mV). Data collection and analysis were performed using custom Igor Pro routines written by R. Lewis (Stanford University). The relative permeability of $Cs^+$ to $Na^+$ was calculated using the relation

$$P_{Cs}/P_{Na} = [Na]_{ext}/[Cs]_{int} e^{-E_{rev}F/RT}, \quad (3)$$

where R, T, and F have their usual meanings, and $E_{rev}$ is the reversal potential. Curve fitting was done using built-in and user-defined functions in Igor Pro (Wavemetrics). All statistical tests were performed using Prism (GraphPad Software).

In a prior study (Yen et al., 2016), many cells displayed excess current noise transiently upon switching between $Ca^{2+}$-containing Ringer's and DVF solutions, and were excluded from analysis as the noise did not appear to be contributed by CRAC channels. Upon further study, we determined that the excess noise was induced by acidification of the extracellular solution when $Ca^{2+}$ in the Ringer's solution transiently mixed with and released protons from the EGTA and HEDTA in the DVF solutions. The noise arose most likely from activation of acid-sensing ion channels, which are endogenous to HEK cells (Gunthorpe et al., 2001). In the current study, we prevented the appearance of excess noise by eliminating HEDTA, reducing [EGTA], and increasing [HEPES] in the $Ca^{2+}$-free DVF Ringer's to minimize pH changes when switching to or from this solution (see Solutions).

### *Noise analysis*

The noise analysis experimental protocol was based on the general method we described previously (Yen et al., 2016) with the following changes. Upon break-in with 20 mM extracellular calcium ($Ca^{2+}_{ext}$), CRAC current was gradually evoked by passive ER store depletion. After current reached a maximum, 200-ms sweeps were collected every 1.25 s at a holding potential of −100 mV, filtered at 2 kHz, and sampled at 5 kHz. DVF solutions containing various free [$Ca^{2+}$] were perfused for 5–10 s followed by a return to 20 mM $Ca^{2+}$ in between DVF perfusion cycles.

Plots of variance ($\sigma^2$) and mean current ($I$) during each 200-ms sweep were fitted with the relation

$$\sigma^2 = Ii - I^2/N, \quad (4)$$

to obtain estimates of $i$, the unitary current, and $N$, the number of channels that can access the open state during the sampling period (Sigworth, 1980). The variance/mean current ratio is related to $P_o$ by the relation

$$\sigma^2/I = i(1 - P_o). \quad (5)$$

Thus, $i$ was also estimated from pooled cell data from a plot of $\sigma^2/I$ versus $1–P_o$, where the slope of the linear fit indicates $i$. After obtaining estimates for $i$ and $N$, the open probability $P_o$ was calculated as

$$P_o = I/(iN). \quad (6)$$

To estimate unitary $Ca^{2+}$ current from unitary $Na^+$ current, we assumed that the ratio of unitary currents should be proportional to the ratio of their macroscopic currents, according to the relation

$$\frac{I_{Ca}}{I_{Na}} = \frac{N_{Ca}}{N_{Na}} \frac{i_{Ca}}{i_{Na}} \frac{P_{o,Ca}}{P_{o,Na}}, \quad (7)$$

where $I$ is the macroscopic current, $N$ is the number of channels, and $P_o$ is their open probability. $P_{o,Ca}/P_{o,Na}$ is given by the extent of CDI in 20 mM $Ca^{2+}$ at −100 mV. Assuming that the number of active channels is constant when the bath is immediately switched from 20 mM $Ca^{2+}$ to $Na^+$-DVF, the relation simplifies to

$$\frac{I_{Ca}}{I_{Na}} = \frac{i_{Ca}}{i_{Na}}(1 - CDI), \quad (8)$$

and, solving for $i_{Ca}$,

$$i_{Ca} = i_{Na} \frac{I_{Ca}}{I_{Na}} \frac{1}{(1 - CDI)}. \quad (9)$$

An example of this conversion has been described in detail (Mullins et al., 2016).

### Antibody staining and flow cytometry

To compare expression across concatemer variants, HEK293-H cells were transfected with equal amounts of concatemer plasmid and maintained under the same conditions used for patch-clamp or imaging experiments. For each variant, 1.5 × $10^6$ cells were incubated with 10 µg/ml 2C1.1 primary mAb (gift from H. McBride, Amgen, Thousand Oaks, CA) in fluorescence-activated cell sorting (FACS) buffer (PBS with 2% FBS) for 45 min at 4°C. 2C1.1 binds specifically to the extracellular 3–4 loop of human Orai1 (Lin et al., 2013). After washing with FACS buffer, cells were resuspended in 3 µg/ml goat anti–human IgG conjugated to Alexa 594 for 20 min at 4°C, washed again in FACS buffer, and fixed in 2% paraformaldehyde for 10 min at 22–25°C. Fixed cells were washed twice with FACS buffer and passed through a 60-µm cell strainer (Becton Dickinson Biosciences) before analysis on a FACScan flow cytometer (Becton Dickinson Biosciences) using the GFP (488 nm excitation, 560 SP splitter, 525 ± 25 nm emission) and Alexa 594 channels (561 nm excitation, 600 SP splitter, 590 ± 10 nm emission). Data were analyzed using Flowjo software (Flowjo LLC), where single cells were selected for analysis based on forward- and side-scatter characteristics. Untransfected 2C1.1-stained cells served as a negative control, and gates were established such that 99% of these cells fell into the GFP-negative and 2C1.1–Alexa 594–negative populations.

### Online supplemental material

Fig. S1 shows that the different Orai1 dimer variants used in Fig. 1 are expressed at comparable levels at the plasma membrane, and

that dimers can assemble in two orientations. Fig. S2 presents a schematic of dimeric versus monomeric STIM1 binding modes. Fig. S3 shows that the mutant constructs used in Figs. 2 and 3 are expressed at the plasma membrane at similar levels as WT hexameric Orai1. Fig. S4 shows the effects of closed channel kinetics on estimates of $N$ and $P_o$ from noise analysis.

## Results

### STIM1 and CAD interact with pairs of Orai1 C termini

For our studies of STIM-Orai binding, we constructed Orai1 channels from tandem concatenated dimers of Orai1, which allowed us to introduce binding site mutations or deletions in selected Orai1 C termini. CFP-labeled Orai1 dimers were coexpressed in HEK293 cells with YFP-labeled STIM1 constructs, and after ER $Ca^{2+}$ depletion with TG, FRET was measured to estimate the degree of binding between the two proteins near the plasma membrane (Fig. 1 A). STIM1 exhibited high FRET with the WT-WT Orai1 dimer, but negligible FRET with the L273D-L273D Orai1 homodimer (Fig. 1 B), as expected from previous studies showing that homomeric L273D channels fail to bind STIM1 in situ (Li et al., 2011; Zhou et al., 2016). The Orai1 dimers were expressed at similar levels as assessed by FACS analysis of cells stained with anti-Orai1 mAb (Fig. S1 A).

Several mutations or deletions in the Orai1 C terminus were tested for their effects on STIM1 binding. Hexameric channels constructed from WT-ΔCT heterodimers (in which one C terminus is deleted) are expected to have only three C termini, and the level of FRET was ~1/2 of the WT-WT level (Fig. 1 B). To address the possibility that the deletion of every other C terminus might impede the proper folding of the WT C termini, we also tested a WT-polymutant Orai1 construct (WT-PolyMut), in which eight mutations (L273/276>D, L286S, R281/289>A, D284/287/291>A) described in previous studies (Navarro-Borelly et al., 2008; Stathopulos et al., 2013) were introduced into one C terminus to fully block binding. WT-PolyMut Orai1 generated the same level of FRET as WT-ΔCT, confirming that the collection of mutations in the polymutant inhibits binding to the same extent as complete truncation of the C terminus, and that the FRET level reflects binding to channels with only three binding sites.

A significantly higher FRET level was observed with WT-L273D heterodimers, approaching the level seen with WT-WT Orai1 (Fig. 1 B). This finding was surprising in light of the lack of binding to channels derived from L273D homodimers, and suggests that although the L273D C terminus by itself does not bind STIM1 appreciably, it can contribute to STIM1 binding when located next to a WT C terminus. A likely explanation for these findings is that L273D reduces the affinity for STIM1 substantially but not completely, and the binding of STIM1 to a WT Orai1 C terminus increases its local concentration enough to promote interaction with the adjacent low-affinity L273D binding site (Fig. S2; see Discussion). These results suggest that STIM1 can interact with pairs of Orai1 C termini.

FRET measurements between CFP-Orai1 dimers and YFP-CAD yielded similar results, demonstrating that the isolated CAD fragment binds to Orai1 in a similar way as the CAD region within full-length STIM1 (Fig. 1 C). We also tested a concatenated dimer

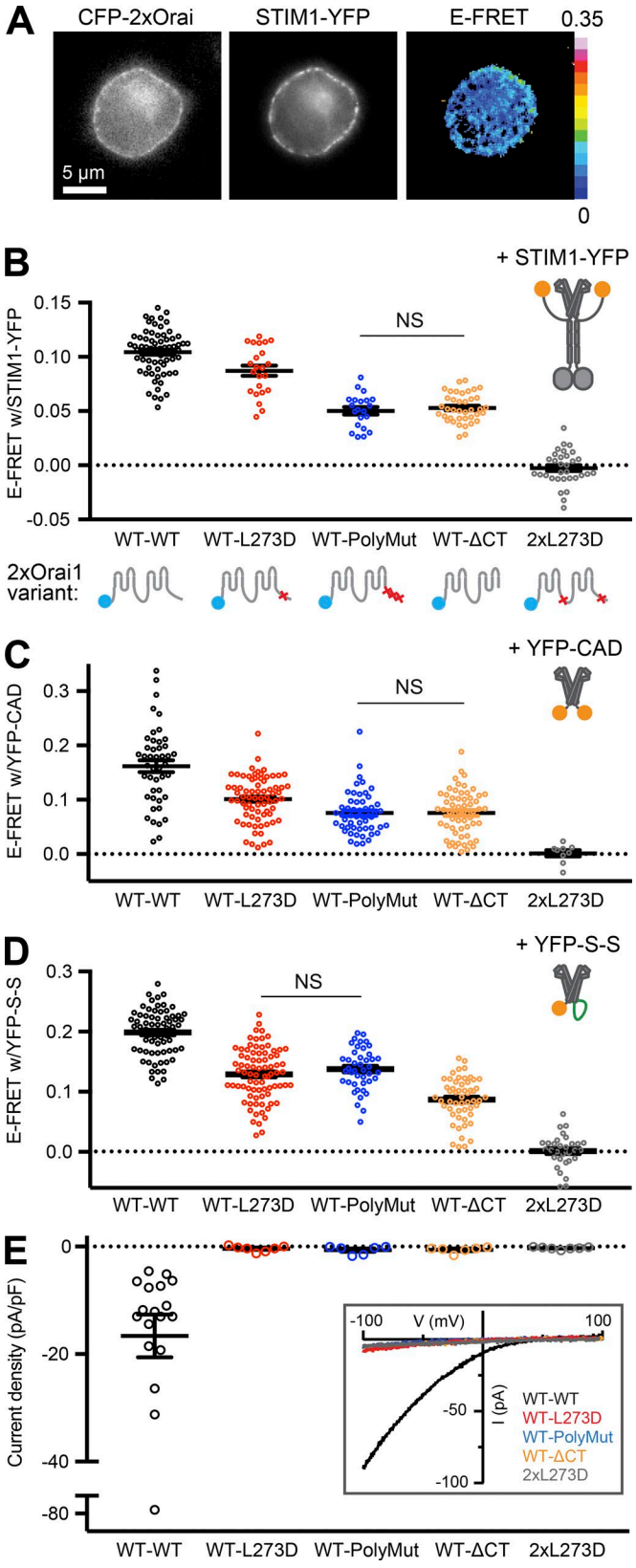


Figure 1. **An L273D Orai1 SU can bind STIM1 only if adjacent to a WT SU.** E-FRET at the plasma membrane was measured between CFP-2xOrai1 and STIM1, CAD, or SOAR concatemers expressed in HEK293 cells. **(A)** Fluorescence and E-FRET images of a cell coexpressing YFP-STIM1 and CFP-2xOrai1, after store depletion by TG treatment. FRET lookup table range, 0–0.35. **(B)**

of SOAR domains (two SOAR domains connected by a 24-residue linker, denoted "S-S") that has been widely used to study STIM1 binding to Orai1 (Li et al., 2011; Palty et al., 2015; Zhou et al., 2015, 2018; Palty and Isacoff, 2016). Given evidence that the non-concatenated CAD fragment assembles as a dimer (Yang et al., 2012), we were surprised to find that the S-S concatenated dimer did not produce the same pattern of FRET levels we observed with STIM1 and CAD (Fig. 1 D). Specifically, the S-S protein bound just as well to WT-PolyMut as to WT-L273D, suggesting that the SOAR concatemer does not interact with Orai1 in the same way as STIM1 or CAD. The altered behavior of the S-S construct may temper its utility for studying the binding mechanism of native STIM1 (see Discussion).

### STIM1 binding to an L273D Orai1 SU contributes to channel activation

Given our finding that the L273D Orai1 SU contributes to STIM1 binding when adjacent to a WT SU, we asked whether the binding to L273D was coupled to channel activation. We initially recorded $Ca^{2+}$ currents elicited by STIM1 binding to the various Orai1 tandem dimers to compare the apparent level of binding (FRET) and channel activation (Fig. 1 E). The WT-WT Orai1 dimer produced current amplitudes (−17 ± 4 pA/pF, $n$ = 18 cells) comparable to those seen after expression of WT Orai1 monomers (−27 ± 4 pA/pF, $n$ = 17 cells), indicating that the linking of Orai1 SUs did not grossly inhibit channel activity. However, none of the Orai1 heterodimers produced detectable currents despite significant binding to STIM1; this is particularly striking in the case of WT-L273D, for which FRET was 83% of WT-WT. This result suggests a highly nonlinear relation between STIM1 binding and channel opening, such that inhibiting STIM1 binding to three SUs within the channel, either partially via the L273D mutation or completely through truncation or polymutation, essentially prevents channel opening.

To evaluate the effect of the L273D mutation on channel activation more quantitatively, we compared the currents produced by hexameric Orai1 concatemers (Yen et al., 2016) in which only one SU was modified with the L273D mutation, the C-terminal truncation, or the PolyMut C terminus. Hereafter we refer to these hexameric constructs as 1xL273D, 1xΔCT, or 1xPolyMut, respectively (Fig. 2 A). When coexpressed with mCherry-STIM1, 1xL273D channels produced ∼35% of the current observed with WT hexamers (Yen et al., 2016). Both the 1xΔCT and the 1xPolyMut currents were smaller than 1xL273D, resulting in ∼20% of the WT level. All three mutants generated I-V relations that were similar to those of WT hexamers (Fig. 2 B). Expression of the Orai1 mutant hexamers at the cell surface as assessed by FACS analysis of cells stained with anti-Orai1 mAb was similar to WT (Fig. S3, A and B), demonstrating that the reduced current levels were not the result of defective expression, assembly, or trafficking to the plasma membrane. Because the 1xL273D currents were on average larger than the 1xPolyMut and 1xΔCT currents, we conclude that the additional STIM1 binding at the L273D site (Fig. 1 B) is functionally coupled to channel activation.

The nonlinear relation between STIM1 binding and channel activity was explored further by introducing multiple mutations of L273D or L286S (a milder inhibitory mutation; Stathopulos et al., 2013) in hexameric Orai1 concatemers that were coexpressed with STIM1. In both mutant series, current declined as an exponential function of the number of STIM1 binding site mutations. Each L273D mutation reduced the current by 64%, while each of the weaker L286S mutations reduced the current by 44% (Fig. 3). The effects of the mutations were independent of their positions in the hexamer, as similar current levels were observed for L273D substitution in SUs 1+2, 2+3, or 1+3 (−1.38 ± 0.07, −2.22 ± 0.55, and −1.59 ± 0.46 pA/pF, respectively; mean ± SEM, $n$ = 7–8 cells per variant; P = 0.431 for one-way ANOVA). FACS analysis showed similar levels of surface expression for each of the mutants, confirming that the declining levels of current were related to differences in channel activity rather than expression (Fig. S3, B and C).

### The L273D mutation strongly affects Orai1 unitary conductance and open probability

The reduced current amplitude of the 1xL273D mutant channel could in principle result from changes in any of several parameters, as the whole-cell current is the product of the number of channels at the PM ($N$), their unitary current amplitude ($i$), and their open probability ($P_o$). The number of 1xL273D channels at the PM ($N$), measured by FACS analysis of mAb binding to an extracellular epitope, was similar to the number of WT hexamers (Fig. S3 B). Because of the extremely low unitary conductance of CRAC channels, $i$ and $P_o$ cannot be assessed directly by patch-clamp recording, but noise analysis can be applied to estimate these parameters from $Na^+$ currents recorded under divalent-free (DVF) conditions. As with other $Ca^{2+}$-selective channels, complete removal of divalent cations from CRAC channels allows monovalent cations to permeate, and addition of micromolar amounts of $Ca^{2+}$ causes transient blocking events that produce current fluctuations at the whole-cell level (Prakriya and Lewis, 2006; Yen et al., 2016). Fig. 4 A shows inward $Na^+$ currents recorded in the presence of 0–342 µM $Ca^{2+}$ from a cell expressing STIM1 and the 1xL273D Orai1 hexamer. Current traces from the same experiment, displayed at a higher time resolution, show fluctuations in the presence of various levels of $Ca^{2+}_{ext}$ (Fig. 4 B). A parabolic fit to a plot of current variance against mean cur-

E-FRET between Orai1 dimer variants and STIM1. Data from individual cells are plotted with means ± SEM. P > 0.99 between WT-ΔCT and WT-PolyMut cells (NS), and P < 0.0001 for all other pairwise comparisons (all P values calculated using one-way ANOVA with Tukey's correction for multiple comparisons). **(C)** E-FRET between Orai1 dimer variants and CAD. P > 0.99 between WT-ΔCT and WT-PolyMut cells; P = 0.0001 between WT-WT and WT-L273D, WT-PolyMut, or WT-ΔCT; and P = 0.02 between WT-L273D and WT-PolyMut or WT-ΔCT. **(D)** E-FRET between Orai1 dimer variants and the dimeric SOAR concatemer (S-S). Unlike STIM1 or CAD, S-S FRETs equally well with WT-PolyMut and WT-L273D. P = 0.75 between WT-L273D and WT-PolyMut cells (NS), and P < 0.0001 for all other pairwise combinations. **(E)** Patch-clamp recordings of currents in 20 mM $Ca^{2+}$ from HEK293 cells expressing full-length mCherry-STIM1 with CFP- or GFP-tagged 2xOrai1 dimer variants after passive store depletion. Peak currents during steps to −100 mV from individual cells are shown with means ± SEM. P < 0.05 for all comparisons between WT-WT and mutant Orai dimers. Representative I-V relations are displayed in the boxed inset.

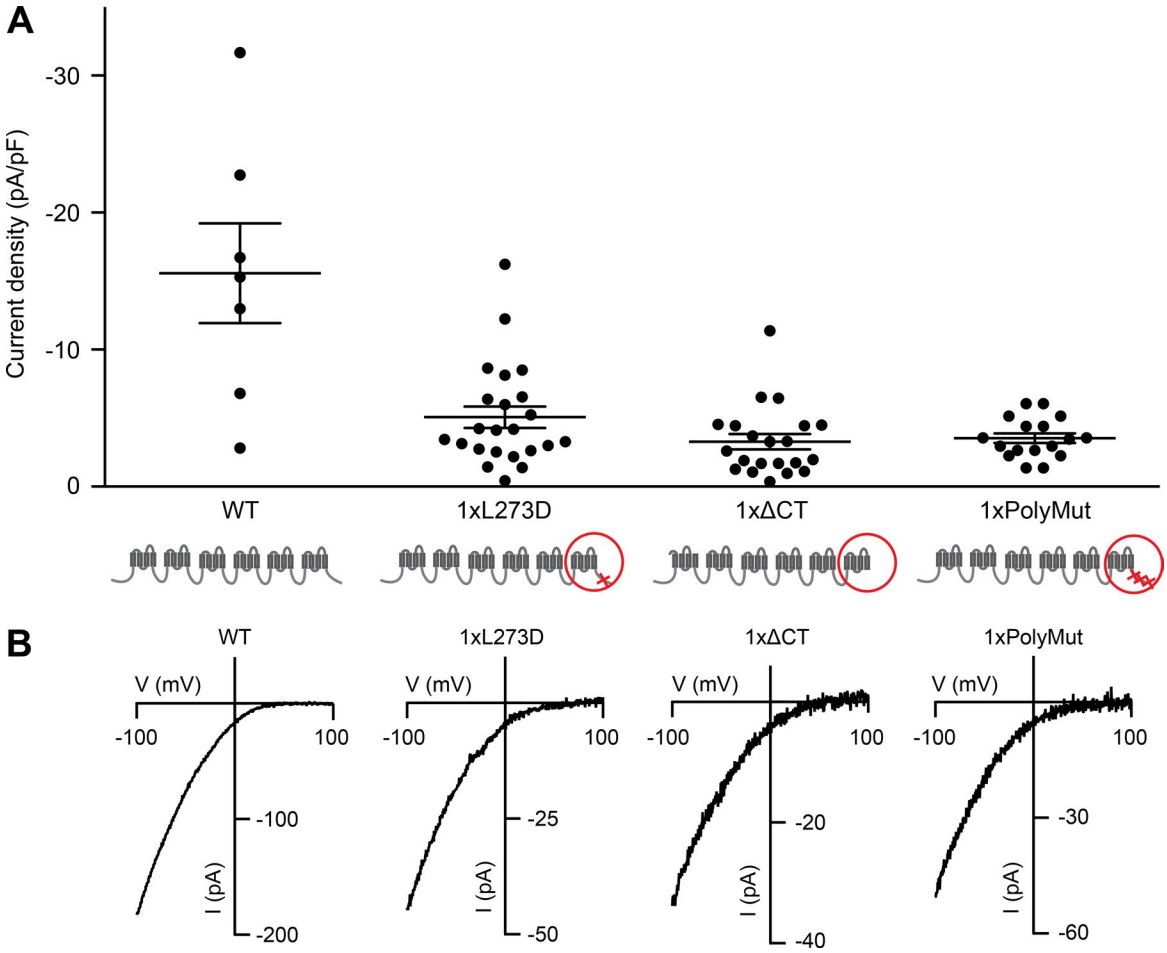


Figure 2. **The L273D Orai1 SU contributes to CRAC channel activation when adjacent to a WT SU.** Whole-cell currents measured at −100 mV in 20 mM $Ca^{2+}$ from HEK293 cells cotransfected with GFP-labeled Orai1 hexameric concatemers and mCherry-STIM1. **(A)** Current densities of individual cells expressing WT, 1xL273D, 1xΔCT, and 1xPolyMut hexamers are displayed with means ± SEM. WT and 1xL273D data are reproduced from a previous publication (Yen et al., 2016) for comparison, and L273D mutants in SUs 1, 3, and 6 were pooled. P = 0.04 between 1xL273D and 1xΔCT, and P > 0.05 between 1xPolyMut and 1xL273D or 1xΔCT (Mann-Whitney *U* test). **(B)** Representative I-V relations of individual cells expressing the indicated hexameric Orai1 variant.

rent yielded estimates for *N*, *i*, and $P_o$ (Fig. 4 C; see Materials and methods). The mutation caused several significant changes relative to WT channels: a moderate reduction of $P_o$ to 0.66 (relative to 0.76 for the WT hexamer), and surprisingly, a large increase in the unitary $Na^+$ current to −321 fA (relative to −81 fA for WT) together with a large decrease in *N* (540 compared with 7,300 for WT). In four 1xL273D cells analyzed individually in this way, mean $i_{Na}$ was −254 ± 28 fA (Table 1), similar to the $i_{Na}$ estimated from pooled values of the variance/mean current ratio versus $1–P_o$ (−248 ± 22 fA; Fig. 4 D). To estimate the unitary $Ca^{2+}$ current, we divided $i_{Na}$ by the ratio of whole-cell $Na^+$ current in DVF to the $Ca^{2+}$ current in 20 mM $Ca^{2+}$, after correcting for the fraction of $Ca^{2+}$ current that was lost at steady-state because of CDI (see Materials and methods; Mullins et al., 2016). The average estimated $i_{Ca}$ of 1xL273D channels from four cells was about three times larger than that of WT (Table 1).

These results show that the reduction of whole-cell $Ca^{2+}$ current produced by the single L273D mutation cannot be explained simply by a reduction in $P_o$ as measured by noise analysis, as it is also affected by a decrease in *N* and an increase in *i*. As developed further in the Discussion, the *N* and $P_o$ values derived from noise analysis only pertain to channels that are able to access the open state during the finite current sampling period. A measure of the true open probability, taking into account the channel's residence in all kinetic states, can be obtained from the relation $P_o = I/Ni$, where *I* and *i* are the whole-cell and unitary currents, respectively, and *N* is the number of channels in the plasma membrane. Thus, we can estimate the true open probability of 1xL273D channels relative to WT channels as

$$\frac{P_{o,\,L273D}}{P_{o,\,WT}} = \frac{I_{L273D}}{I_{WT}} \frac{N_{WT}^{PM}}{N_{L273D}^{PM}} \frac{i_{WT}}{i_{L273D}}, \quad (10)$$

where the subscripts indicate WT or 1xL273D channels, and $N^{PM}$ is the number of channels in the plasma membrane. The *N*s cancel because their expression is equal (Fig. S3 B), and after substituting values for *I* (Fig. 2 A) and *i* (Table 1), we estimate that the true $P_o$ of 1xL273D relative to WT hexamers is 0.12. Thus, the true $P_o$ for 1xL273D is considerably smaller than the value estimated from noise analysis (0.56), which describes the fraction of channels that can access the open state during the sampling period. This difference in $P_o$ values implies that STIM1 binding drives CRAC channels through multiple closed states on the way

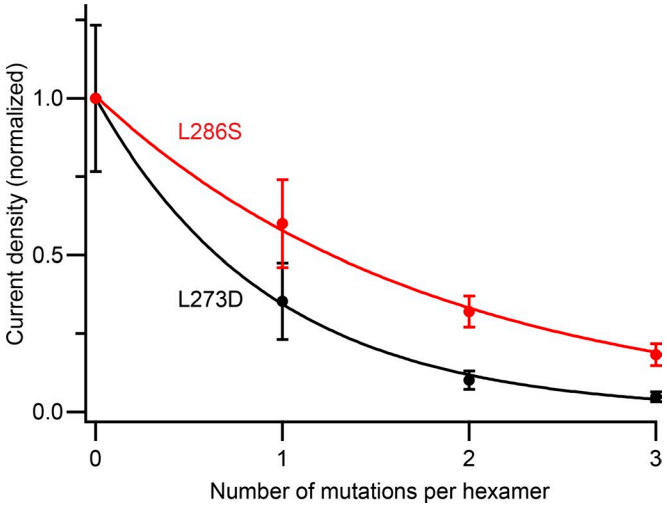


Figure 3. **Relationship between current amplitude and the number of L273D and L286S mutations.** Current densities of HEK293 cells coexpressing GFP-labeled Orai1 hexameric concatemers and mCherry-STIM1 were recorded as in Fig. 2, normalized to that of WT (0 mutations per hexamer, −15.6 pA/pF) and plotted as a function of mutations per channel. WT and 1xL273D values are reproduced from Yen et al. (2016). Each filled circle represents the mean ± SEM of 7–23 cells for the specified hexamer variant. The corresponding solid lines describe exponential fits given by $I = k^n$, where $I$ is the normalized current amplitude, $n$ is the number of mutations, and $k$ is the fractional activity for a single mutation (0.36 for L273D and 0.56 for L286S). For L273D mutations, data were pooled for single mutants made in SUs 1, 3, and 6, double mutants in SU1+2, 2+3, and 1+3, and triple mutants in SU1+3+6. For L286S, the single mutation was placed in SU1, double mutation in SU1+3, and triple mutation in SU1+3+6.

to opening (see Discussion). Most importantly, these results reveal an extremely high sensitivity of CRAC channel activation and unitary conductance to the extent of STIM1 binding, with full binding being required to open the channel significantly as well as to specify its unusually low unitary conductance.

### The L273D mutation reduces the ion selectivity of the Orai1 channel

In addition to increasing the unitary conductance, the L273D mutation induced other changes in Orai1 pore properties. The $Ca^{2+}$ blocking affinity of 1xL273D channels was reduced ($K_{1/2}$ = 47 ± 8 μM) relative to the WT hexamer ($K_{1/2}$ = 16 ±3 μM; Table 1; see also Fig. 4 E), implying a change in the configuration of the selectivity filter. $Ca^{2+}$ selectivity of the 1xL273D channel was assessed from I-V relations in the presence and absence of extracellular $Na^+$. In the presence of 2 mM $Ca^{2+}$, substitution of $Na^+$ with NMDG did not affect the I-V relation of WT or 1xL273D channels (Fig. 5, A and B). This result, together with the absence of significant outward current at positive potentials, demonstrates a high selectivity for $Ca^{2+}$ over monovalent cations in both channels. However, under DVF conditions, 1xL273D channels showed a reduced selectivity for $Na^+$ over $Cs^+$ (Fig. 5 C). The reversal potential of 1xL273D channels was 25.9 ± 2.0 mV (mean ± SEM, $n$ = 5) compared with 45.8 ± 1.2 mV for WT channels, corresponding to an increase in the permeability ratio $P_{Cs}/P_{Na}$ to 0.39 relative to 0.16 reported previously for WT channels (Yen et al., 2016). Whereas weakening a single STIM1 binding site did not affect the channel's selectivity for $Ca^{2+}$ over monovalent cations, presumably because the 2 mM $Ca^{2+}_{ext}$ far exceeded the $Ca^{2+}$ pore affinity, it significantly reduced the selectivity for $Na^+$ over $Cs^+$. Thus, ion selectivity, like channel opening, is a highly sensitive function of the extent of STIM1 binding.

## Discussion

The use of Orai1 concatemers to control STIM1 binding to selected Orai1 SUs within the CRAC channel offers new insights about how STIM1 interacts with Orai1 and how the extent of binding affects CRAC channel activity and ion selectivity. Our results reveal that the L273D mutation, which is widely considered to completely prevent binding, can actually add to both binding and channel activation if present next to a WT Orai1 SU, suggesting that STIM1 can interact with pairs of adjacent Orai1 C termini. We also find that CRAC channel activity as well as its characteristic unitary conductance and selectivity are all unexpectedly sensitive functions of STIM1 binding.

### STIM1 interacts with pairs of Orai1 C termini

For these studies, we used the E-FRET method (Zal and Gascoigne, 2004) to estimate the degree of binding between STIM1 and Orai1. This method measures the quenching of CFP-Orai1 by YFP fused to STIM1, CAD, or SOAR concatemers. A potential caveat of this approach is that the separation and dipole orientations of the fluorescent proteins could affect FRET efficiency independently of the number of STIMs bound. However, two lines of evidence argue that the FRET levels reflect relative degrees of binding. First, the patterns of FRET levels for STIM1 and CAD bound to the different mutant CFP-Orai1 proteins were similar even though the positions of the YFP attachment sites on STIM1 and CAD were quite distinct and therefore likely to assume different locations and orientations relative to CFP-Orai1. Second, in hexameric Orai1 concatemers, the L273D SU increased current amplitude relative to PolyMut or ΔCT Orai1 SUs, consistent with its enhancing effect on FRET and illustrating its ability to interact functionally with STIM1.

Our FRET measurements with the Orai1 WT-L273D dimer indicate that STIM1 or CAD can interact with two adjacent Orai1 SUs. The L273D mutation is widely considered to completely prevent STIM1 binding as judged by its ability to inhibit Orai1 coclustering with STIM1, FRET between STIM1 and Orai1, and Orai1 channel activation (Li et al., 2011; Zhou et al., 2016, 2018; Vaeth et al., 2017). Consistent with this notion, the Orai1 L273D-L273D mutant did not FRET appreciably with STIM1 or CAD or produce measurable current (Fig. 1). However, placing the L273D mutant SU next to a WT SU enhanced binding relative to WT-ΔCT or WT-PolyMut channels, suggesting that the L273D C terminus does in fact have a finite affinity for STIM1. Furthermore, the enhanced binding contributed by L273D translates into increased channel activity (Fig. 2 A), showing that the interaction is functional. Although these data appear to contradict the apparent lack of binding by the L273D homodimer, they may be explained by an increased local concentration of STIM1 afforded by binding to the adjacent WT Orai1 C terminus. Two possible explanations for how STIM1 might "sense" two adjacent C termini

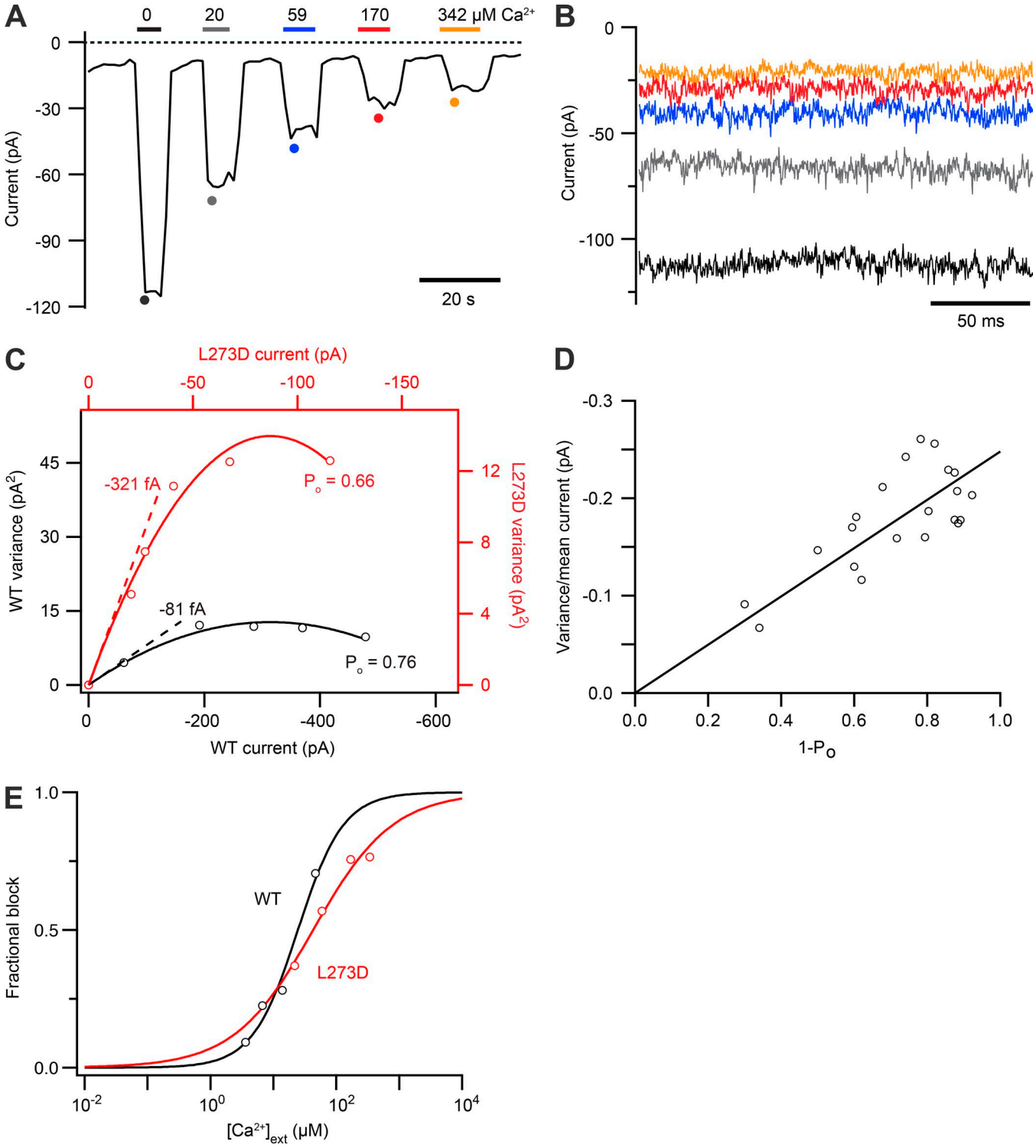


Figure 4. **Noise analysis of Orai1 channels carrying a single L273D mutation. (A)** A cell coexpressing 1xL273D Orai1 hexamer + mCherry-STIM1 was store-depleted and briefly exposed to DVF solutions containing differing free $[Ca^{2+}]_{ext}$ to cause graded block of CRAC channels (colored bars). Current was measured at −100 mV, and cells were returned to 20 mM $Ca^{2+}$ between DVF exposures. **(B)** 200-ms sweeps collected at the times indicated by the corresponding colored dots in A. **(C)** Variance versus mean current plots in two cells expressing WT (black) or 1xL273D (red) Orai1 hexamers. The curves show the best fits of $\sigma^2 = Ii - I^2/N$ to the data, with N ~7,300 and 540, and $i$ = −81 and −321 fA for WT and 1xL273D channels, respectively. Data from the WT cell are reproduced from Yen et al. (2016). Dashed lines indicate $i$ values corresponding to the variance/current slope at the limit of maximum block ($P_o$ = 0). Maximum $P_o$ values in DVF calculated as $I/Ni$ are indicated for each cell. **(D)** Estimating unitary $Na^+$ current through the 1xL273D Orai1 hexamer. Pooled data from four cells shows that $\sigma^2$/mean current increases linearly with $1\text{-}P_o$ with a slope of −248 ± 22 fA (95% confidence limits, $r^2$ = 0.75) indicating the unitary current amplitude. **(E)** $Ca^{2+}$ block of $Na^+$ current in two cells expressing WT (black) or 1xL273D Orai1 hexamers (red). Lines represent fits to the Hill equation, $block = 1/[1 + (K_{1/2}/[Ca])^{n_H}]$. $K_{1/2}$ was 25 and 42 µM, with a Hill coefficient ($n_H$)of 1.2 and 0.7 for WT and 1xL273D channels, respectively.

Table 1. **Unitary properties and $Ca^{2+}$ affinity of WT and single L273D channels derived from hexameric Orai1 concatemers**

| Channel | $P_o$ | N | $i_{Na}$(fA) | $i_{Ca}$ (fA) | $Ca^{2+}$ affinity ($K_{1/2}$, μM) | Hill coefficient ($n_H$) |
|---|---|---|---|---|---|---|
| WT[a,b] | 0.76 ± 0.04 | 8,339 ± 1,725 | −87 ± 7 | −19 ± 2 | 16 ± 3 | 1.15 ± 0.02 |
| 1xL273D[a] | 0.56 ± 0.08 | 730 ± 157 | −254 ± 28 | −53 ± 10 | 47 ± 8 | 0.73 ± 0.05 |
| P value[c] | 0.057 | 0.029 | 0.029 | 0.019 | 0.016 | 0.016 |

Mean values ± SEM $n$ = 4 cells for WT, 4–5 cells for 1xL273D.
[a]Channel properties measured at −100 mV.
[b]Values reproduced from Yen et al. (2016).
[c]P values determined by Mann-Whitney unpaired $t$ test.

are diagrammed in Fig. S2. In the first scenario, a STIM1 dimer engages both C termini simultaneously (dimeric binding), an example of which is the complex of STIM1 and Orai1 fragments described by Stathopulos et al. (2013). In the second scenario, STIM1 binds reversibly in a monomeric fashion to the WT C terminus as suggested by Zhou et al. (2015), and upon unbinding, interacts transiently with the nearby L273D helix (a monomeric "hop" mechanism). In each case, the high local concentration resulting from binding to the WT SU would be expected to promote interactions with the low-affinity L273D neighbor. For both models, it is also possible that initial binding of STIM1 to the WT SU could allosterically increase the affinity of the neighboring L273D SU for STIM1, perhaps through structural rearrangements of the Orai1 C terminus (Palty et al., 2017). Definitively distinguishing between the monomeric and dimeric binding modes will require structural studies of the STIM1-Orai1 complex or approaches capable of resolving real-time interactions of a single STIM1 dimer with a pair of C termini to determine whether the interactions are simultaneous or sequential.

A recent study used concatenated dimers of SOAR domains to support a monomeric binding model in which only one SU of each STIM1 (or SOAR) dimer binds to each Orai1 SU (Zhou et al., 2015). However, we found that the concatenated SOAR dimer (S-S) appears to engage Orai1 C termini in a different manner than nonconcatenated CAD or STIM1. Relative to the Orai1 WT-ΔC dimer, the WT-PolyMut dimer enhanced binding of the S-S concatemer to the same extent as WT-L273D, but it did not enhance the binding of STIM1 or CAD (Fig. 1, B–D). A likely explanation for this discrepancy is that SOAR concatemers engage a different binding interface than CAD or native STIM1, specifically one that is insensitive to mutant residues downstream of L273 (the polymutant comprises mutations at L273 and seven more C-terminal residues). These results suggest that SOAR concatemers may not precisely mimic native STIM1 binding, perhaps because the 24-aa linker between the SOAR SUs restricts conformational flexibility. Similar dimeric SOAR concatemers have been widely used to study STIM-Orai binding and activation (Li et al., 2011; Palty et al., 2015; Zhou et al., 2015, 2018; Palty and Isacoff, 2016). Our results suggest caution in using these concatemers to make strong inferences about the binding mechanism of native STIM1.

The FRET we observed between STIM/CAD and channels assembled from WT-ΔCT or WT-PolyMut Orai1 dimers in Fig. 1 appears to indicate STIM1 binding to single Orai1 C termini, assuming that the Orai1 dimers assemble in a fixed order to gener-

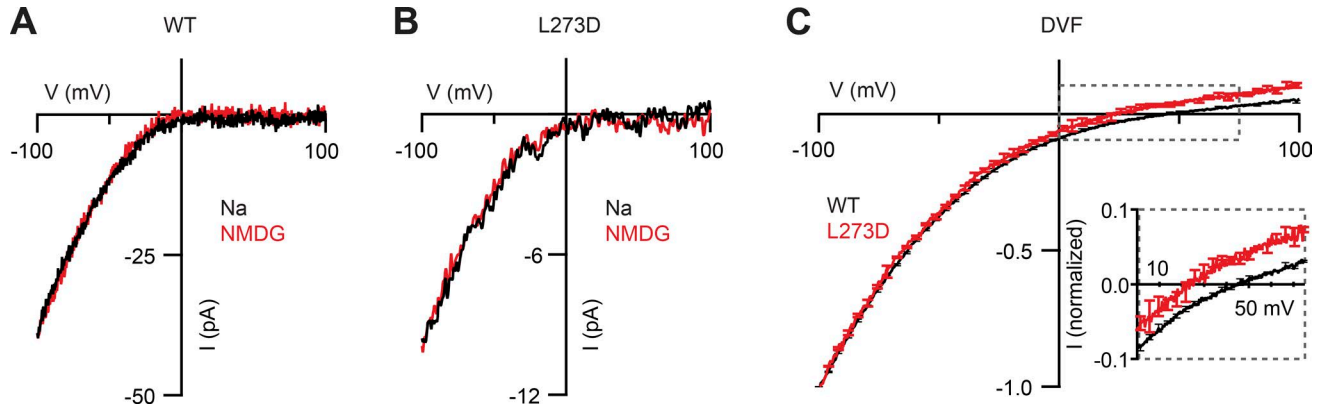


Figure 5. **Ion selectivity of L273D currents.** I-V relations of hexameric WT and 1xL273D channels in cells coexpressing mCherry-STIM1. Selectivity in physiological $Ca^{2+}$ was assessed in 2 mM $Ca^{2+}$ Ringer's, in the presence of extracellular $Na^+$ (*black*) or after replacement of $Na^+$ by NMDG (red). Exemplar I-V relations of a cell coexpressing mCherry-STIM1 with WT **(A)** or 1xL273D **(B)** hexamer channels. No change was observed when extracellular $Na^+$ was removed, indicating that $Na^+$ does not permeate either WT or 1xL273D channels. **(C)** I-V relations in DVF Ringer's from WT (black) or 1xL273D (red) channels were normalized to their peak current at −100 mV and averaged ($n$ = 3–4 cells per variant). The SEM is plotted for every 10th point. $E_{rev}$ was reduced in 1xL273D cells (25.9 ± 2.0 mV compared with 45.8 ± 1.2 mV in WT cells; see inset), indicating an increased $Cs^+$ to $Na^+$ permeability. The average I-V relation for WT Orai1 hexamer is reproduced from Yen et al. (2016) for comparison.

ate channels with a SU pattern of WT-mut-WT-mut-WT-mut. To assess the order of assembly, we applied a cross-linking method based on the ability of adjacent L273C Orai1 SUs to form disulfide cross-links under oxidizing conditions (Tirado-Lee et al., 2015). As expected, L273C channels assembled from Orai1(L273C) monomers were cross-linked to form dimers in a diamide-dependent manner (Fig. S1 B). However, when an L273C mutation was introduced into the WT SU of the WT-PolyMut Orai1 dimer, diamide cross-linked the dimers to form tetramers. This result indicates some degree of random ordering to generate channels with a pair of adjacent L273C SUs (e.g., L273C-PolyMut-PolyMut-L273C-L273C-PolyMut). Thus, we expect WT-PolyMut and WT-ΔC dimers to produce channels with adjacent WT SUs, and therefore the FRET we observed with those constructs cannot be unequivocally ascribed to monomeric binding. These results underscore the importance of testing assumptions about how protein concatemers assemble to form channels (Sack et al., 2008).

### Full binding of STIM1 to Orai1 is required to effectively activate the CRAC channel

The relationship between the number of STIM1s bound and channel activity is not well understood. Previous studies approached this question using mutant Orai1 concatemers or by varying the expression ratios of STIM1 and Orai1. In one study in which L273D was introduced into one to four SUs of a tetrameric Orai1 concatemer, activation was graded with the number of mutations, with each L273D reducing the current level by a factor of ∼0.5 (Li et al., 2011). This value is slightly greater than the reduction factor of 0.36 we found for each L273D mutation in hexameric concatemers, but a detailed comparison is complicated by the fact that Orai1 is now considered to assemble as a hexamer (Hou et al., 2012; Cai et al., 2016; Yen et al., 2016), and the SU stoichiometry of channels made from tetrameric concatemers is not clear.

Our results suggest that CRAC channel opening is not smoothly graded with the number of STIM1s bound as implied by current amplitudes, but rather is steeply dependent on binding such that all six Orai1 SUs must be occupied for significant activation. This conclusion follows from the fact that a single L273D mutation induces a threefold increase in the single-channel current, so that the open probability of the mutant channel is actually three times lower than predicted by the whole-cell current, or only ∼10% of WT. The open probability of channels with a complete loss of STIM1 binding to one SU (1xΔCT or 1xPolyMut) is likely to be even lower, considering that the 1xΔCT and 1xPolyMut mutants produce less current (Fig. 2) and may have a higher unitary conductance than the 1xL273D channel. Finally, the $P_o$ values we obtained are relative to that of WT channels, which is less than 1 (noise analysis estimates an upper limit of 0.8), further reducing the absolute $P_o$ of the mutant channels. Collectively, these results suggest that all six SUs must engage STIM1 in order to effectively open the gate.

These new findings are consistent with an earlier study in which we assessed $I_{CRAC}$ amplitude in response to varying the ratio of STIM1 to Orai1 at ER-PM junctions (Hoover and Lewis, 2011). In that study, we inferred a high degree of activation nonlinearity based on an abrupt decline in current when the STIM1:Orai1 protein ratio fell below ∼2. Because only total rather than bound protein levels were measured, it was not possible to attribute specific open probabilities to defined binding stoichiometries. However, based on the behavior of the 1xL273D channel, the small currents observed at low STIM1:Orai1 ratios were likely produced by subliganded channels with a very low open probability but increased unitary conductance.

### Implications from noise analysis: Additional closed states for the CRAC channel

The tiny unitary conductance (20–40 femtosiemens) of the CRAC channel poses a serious obstacle to understanding gating transitions and kinetics because single-channel currents are far too small to detect with patch-clamp techniques (Zweifach and Lewis, 1993; Prakriya and Lewis, 2006). However, current fluctuation analysis offers some clues. We found that the effect of the L273D mutation on $N$ and $P_o$ depended on how these parameters were measured. The true value of $N$ is the total number of PM-localized channels, and $P_o$ (calculated as $I/Ni$) gives their mean open probability. Noise analysis should provide these same values assuming that activation can be described by a simple two-state C↔O mechanism (Sigworth, 1980). However, the two methods yielded very different values of $N$ and $P_o$. As described below, these discrepancies can be attributed to the presence of additional closed states and a finite current sampling period. A simple kinetic scheme consistent with our data is

$$C_n \leftrightarrow C_n^* \leftrightarrow O_n, \tag{11}$$

where $C$ and $O$ denote closed and open states, $n$ indicates the number of occupied STIM1 binding sites on the channel, and $C_n^*$ represents one or more conformational states leading to opening. Our results suggest that only channels with five or six occupied sites open, and that there are two functionally distinct open states, with the $O_5$ state having increased conductance and reduced selectivity relative to the fully STIM1-bound $O_6$ state.

Because channels produce current only when open, noise estimates of $N$ and $P_o$ describe only the subset of channels that are open and the average fraction of time spent open during the sampling period. If equilibration among closed states is fast relative to the current sample duration, noise analysis will provide an accurate estimate of the true values of $N$ and $P_o$. However, if equilibration among the $C_n$ closed states is slow enough that some channels cannot open during the sampling period, the apparent value of $N$ will be reduced; likewise, $P_o$ will be increased because of biased sampling of channels close to (and able to reach) the open state (Fig. S4). The $N$ value for 1xL273D estimated from noise analysis was 9% of the $N$ value for WT Orai1 hexamers (Table 1). This implies that at least 90% of the mutant channels are in closed states not accessible to the open state during the 200-ms sampling period. Accordingly, 1xL273D reduced the true open probability to 12% of WT, whereas the noise analysis estimate was much higher (74% of WT). This discrepancy arises because noise analysis counts only the fraction of channels that are able to open, and they have a higher $P_o$ because on average they are nearer to the open state. Interestingly, this interpretation of the results suggests that the mutation (and hence STIM1 binding) affects most strongly the speed and/or probability of early transitions in the path from closed to open (i.e., $C_n \leftrightarrow C_n^*$).

This gating scheme is of course greatly oversimplified, but we believe it is a useful starting point for thinking about how STIM1 ultimately drives CRAC channel opening. Further tests of this model may be possible once more is known about the conformational intermediates that couple STIM1 binding to channel opening, and if single-channel currents can be measured using mutant channels with higher conductances.

### Full STIM1 binding is required to produce characteristic CRAC channel pore properties

An unusual feature of the CRAC channel is that STIM1 binding not only opens the channel, but also confers its characteristically high $Ca^{2+}$ selectivity (Scrimgeour et al., 2009; McNally et al., 2012). In this sense, STIM1 serves not merely as an activating ligand but also as a channel SU that assembles with the pore-forming Orai1 SU after store depletion. Constitutively active Orai1 V102C mutant channels have an enlarged pore diameter and reduced selectivity, both of which are normalized by STIM1 binding (McNally et al., 2012). Similarly, channels activated by substoichiometric amounts of STIM1 (Orai1 chimeras with a single attached SOAR domain, or Orai1 expressed at a ratio of 4:1 relative to STIM1) display reduced selectivity for $Ca^{2+}$ and under DVF conditions for $Na^+$ over $Cs^+$ (McNally et al., 2012). These pioneering studies all examined the effects of large deficits of STIM1. Interestingly, we have found that weakening only a single STIM1 binding site elicits multiple effects on ion permeation, including a reduction of $Ca^{2+}$ binding affinity and selectivity for $Na^+$ over $Cs^+$, while greatly increasing the unitary conductance. These results reveal the extreme sensitivity with which STIM1 binding is coupled to permeation: that all six binding sites need to be occupied to configure the pore to generate the characteristic properties of the native CRAC channel.

The altered pore properties of the 1xL273D channels point to a second open state that is accessible when less than the full complement of Orai1 binding sites is occupied. At least some properties of this state may be explained by a recently proposed helical twist model for the coupling of CRAC channel gating and selectivity (Yamashita et al., 2017). According to this model, channel opening occurs by a rotation of hydrophobic F99 residues out of the pore, allowing water to enter and relieve the hydrophobic block of $Ca^{2+}$ permeation. Increased affinity of the $Ca^{2+}$ binding site in the selectivity filter is thought to result from a coupled rotation of the E106 side chains located two turns above F99 in the TM1 helix. Viewed in terms of this model, the low $P_o$ and reduced $Ca^{2+}$ affinity of the L273D mutant may therefore result from incomplete rotation of one or more helices in the outer pore region. The structural basis of the channel's low conductance and low permeability to $Cs^+$ is unknown, but may involve domains distinct from E106 and F99. Thus, full STIM1 binding may also be required to establish the configuration of other pore regions that limit $Cs^+$ permeability and unitary CRAC channel conductance.

The steep dependence of CRAC channel gating and permeation on STIM1 binding has important implications for store-operated calcium entry under physiological conditions. Upon ER $Ca^{2+}$ release and store depletion, CRAC channels accumulate at ER-PM junctions, where they bind increasing amounts of STIM1. Because channels near the threshold for opening (with five sites occupied) retain the ability to exclude $Na^+$, they will conduct mostly $Ca^{2+}$ from the time they first open. Minimizing $Na^+$ influx-dependent depolarization will also help maintain the driving force for $Ca^{2+}$ entry, further promoting $Ca^{2+}$ influx over a range of stimulus intensities. The high level of STIM1 binding required to open the CRAC channel raises the possibility that the time needed to reach a threshold of STIM1 binding, together with STIM1 and Orai1 diffusion rates, may help determine the characteristically slow activation kinetics of CRAC current. Further studies of the STIM1 binding mechanism, including the stoichiometry and cooperativity of binding, will help identify the essential parameters that shape the time course and amplitude of CRAC channel activation after store depletion.

## Acknowledgments

The authors thank Rick Aldrich and members of the Lewis laboratory for helpful discussions; Stijn van Dorp for insights into noise analysis; Luda Lokteva for assistance with constructing plasmids; Don Gill, Helen McBride, Chan Young Park, and Tao Xu for antibodies and plasmids; and Vladimir Avodnin and Toshi Hoshi for PatchMachine software.

This work was supported by National Institutes of Health MERIT award R37GM45374 and the Mathers Charitable Foundation (to R.S. Lewis). M. Yen's training was supported by the National Science Foundation Graduate Research Fellowship Program and National Institutes of Health training grant 5T32AI007290 to the Stanford Immunology Graduate Program.

The authors declare no competing financial interests.

Author contributions: M. Yen performed all experiments and prepared the figures; M. Yen and R.S. Lewis designed the experiments, analyzed the data, and wrote and edited the manuscript.

Eduardo Ríos served as editor.

Submitted: 22 December 2017
Revised: 8 June 2018
Accepted: 30 July 2018

## References

Blanchetot, C., L.G.J. Tertoolen, and J. den Hertog. 2002. Regulation of receptor protein-tyrosine phosphatase alpha by oxidative stress. *EMBO J.* 21:493–503. https://doi.org/10.1093/emboj/21.4.493

Cai, X., Y. Zhou, R.M. Nwokonko, N.A. Loktionova, X. Wang, P. Xin, M. Trebak, Y. Wang, and D.L. Gill. 2016. The Orai1 store-operated calcium channel functions as a hexamer. *J. Biol. Chem.* 291:25764–25775. https://doi.org/10.1074/jbc.M116.758813

Gunthorpe, M.J., G.D. Smith, J.B. Davis, and A.D. Randall. 2001. Characterisation of a human acid-sensing ion channel (hASIC1a) endogenously expressed in HEK293 cells. *Pflugers Arch.* 442:668–674. https://doi.org/10.1007/s004240100584

Hirve, N., V. Rajanikanth, P.G. Hogan, and A. Gudlur. 2018. Coiled-coil formation conveys a STIM1 signal from ER lumen to cytoplasm. *Cell Reports.* 22:72–83. https://doi.org/10.1016/j.celrep.2017.12.030

Hoover, P.J., and R.S. Lewis. 2011. Stoichiometric requirements for trapping and gating of $Ca^{2+}$ release-activated $Ca^{2+}$ (CRAC) channels by stromal interaction molecule 1 (STIM1). *Proc. Natl. Acad. Sci. USA.* 108:13299–13304. https://doi.org/10.1073/pnas.1101664108

Hoth, M. 1995. Calcium and barium permeation through calcium release-activated calcium (CRAC) channels. *Pflugers Arch.* 430:315–322. https://doi.org/10.1007/BF00373905

Hou, X., L. Pedi, M.M. Diver, and S.B. Long. 2012. Crystal structure of the calcium release-activated calcium channel Orai. *Science.* 338:1308–1313. https://doi.org/10.1126/science.1228757

Kawasaki, T., I. Lange, and S. Feske. 2009. A minimal regulatory domain in the C terminus of STIM1 binds to and activates ORAI1 CRAC channels. *Biochem. Biophys. Res. Commun.* 385:49–54. https://doi.org/10.1016/j.bbrc.2009.05.020

Li, Z., J. Lu, P. Xu, X. Xie, L. Chen, and T. Xu. 2007. Mapping the interacting domains of STIM1 and Orai1 in $Ca^{2+}$ release-activated $Ca^{2+}$ channel activation. *J. Biol. Chem.* 282:29448–29456. https://doi.org/10.1074/jbc.M703573200

Li, Z., L. Liu, Y. Deng, W. Ji, W. Du, P. Xu, L. Chen, and T. Xu. 2011. Graded activation of CRAC channel by binding of different numbers of STIM1 to Orai1 subunits. *Cell Res.* 21:305–315. https://doi.org/10.1038/cr.2010.131

Lin, F.F., R. Elliott, A. Colombero, K. Gaida, L. Kelley, A. Moksa, S.Y. Ho, E. Bykova, M. Wong, P. Rathanaswami, et al. 2013. Generation and characterization of fully human monoclonal antibodies against human Orai1 for autoimmune disease. *J. Pharmacol. Exp. Ther.* 345:225–238. https://doi.org/10.1124/jpet.112.202788

Liou, J., M.L. Kim, W.D. Heo, J.T. Jones, J.W. Myers, J.E. Ferrell Jr., and T. Meyer. 2005. STIM is a $Ca^{2+}$ sensor essential for $Ca^{2+}$-store-depletion-triggered $Ca^{2+}$ influx. *Curr. Biol.* 15:1235–1241. https://doi.org/10.1016/j.cub.2005.05.055

Luik, R.M., M.M. Wu, J. Buchanan, and R.S. Lewis. 2006. The elementary unit of store-operated $Ca^{2+}$ entry: local activation of CRAC channels by STIM1 at ER-plasma membrane junctions. *J. Cell Biol.* 174:815–825. https://doi.org/10.1083/jcb.200604015

Luik, R.M., B. Wang, M. Prakriya, M.M. Wu, and R.S. Lewis. 2008. Oligomerization of STIM1 couples ER calcium depletion to CRAC channel activation. *Nature.* 454:538–542. https://doi.org/10.1038/nature07065

Ma, G., M. Wei, L. He, C. Liu, B. Wu, S.L. Zhang, J. Jing, X. Liang, A. Senes, P. Tan, et al. 2015. Inside-out $Ca^{2+}$ signalling prompted by STIM1 conformational switch. *Nat. Commun.* 6:7826. https://doi.org/10.1038/ncomms8826

McNally, B.A., A. Somasundaram, M. Yamashita, and M. Prakriya. 2012. Gated regulation of CRAC channel ion selectivity by STIM1. *Nature.* 482:241–245. https://doi.org/10.1038/nature10752

Mullins, F.M., M. Yen, and R.S. Lewis. 2016. Orai1 pore residues control CRAC channel inactivation independently of calmodulin. *J. Gen. Physiol.* 147:137–152. https://doi.org/10.1085/jgp.201511437

Navarro-Borelly, L., A. Somasundaram, M. Yamashita, D. Ren, R.J. Miller, and M. Prakriya. 2008. STIM1-Orai1 interactions and Orai1 conformational changes revealed by live-cell FRET microscopy. *J. Physiol.* 586:5383–5401. https://doi.org/10.1113/jphysiol.2008.162503

Palty, R., and E.Y. Isacoff. 2016. Cooperative binding of stromal interaction molecule 1 (STIM1) to the N and C termini of calcium release-activated calcium modulator 1 (Orai1). *J. Biol. Chem.* 291:334–341. https://doi.org/10.1074/jbc.M115.685289

Palty, R., C. Stanley, and E.Y. Isacoff. 2015. Critical role for Orai1 C-terminal domain and TM4 in CRAC channel gating. *Cell Res.* 25:963–980. https://doi.org/10.1038/cr.2015.80

Palty, R., Z. Fu, and E.Y. Isacoff. 2017. Sequential steps of CRAC channel activation. *Cell Reports.* 19:1929–1939. https://doi.org/10.1016/j.celrep.2017.05.025

Park, C.Y., P.J. Hoover, F.M. Mullins, P. Bachhawat, E.D. Covington, S. Raunser, T. Walz, K.C. Garcia, R.E. Dolmetsch, and R.S. Lewis. 2009. STIM1 clusters and activates CRAC channels via direct binding of a cytosolic domain to Orai1. *Cell.* 136:876–890. https://doi.org/10.1016/j.cell.2009.02.014

Prakriya, M., and R.S. Lewis. 2006. Regulation of CRAC channel activity by recruitment of silent channels to a high open-probability gating mode. *J. Gen. Physiol.* 128:373–386. https://doi.org/10.1085/jgp.200609588

Prakriya, M., and R.S. Lewis. 2015. Store-operated calcium channels. *Physiol. Rev.* 95:1383–1436. https://doi.org/10.1152/physrev.00020.2014

Prakriya, M., S. Feske, Y. Gwack, S. Srikanth, A. Rao, and P.G. Hogan. 2006. Orai1 is an essential pore subunit of the CRAC channel. *Nature.* 443:230–233. https://doi.org/10.1038/nature05122

Rana, A., M. Yen, A.M. Sadaghiani, S. Malmersjö, C.Y. Park, R.E. Dolmetsch, and R.S. Lewis. 2015. Alternative splicing converts STIM2 from an activator to an inhibitor of store-operated calcium channels. *J. Cell Biol.* 209:653–669. https://doi.org/10.1083/jcb.201412060

Sack, J.T., O. Shamotienko, and J.O. Dolly. 2008. How to validate a heteromeric ion channel drug target: assessing proper expression of concatenated subunits. *J. Gen. Physiol.* 131:415–420. https://doi.org/10.1085/jgp.200709939

Scrimgeour, N., T. Litjens, L. Ma, G.J. Barritt, and G.Y. Rychkov. 2009. Properties of Orai1 mediated store-operated current depend on the expression levels of STIM1 and Orai1 proteins. *J. Physiol.* 587:2903–2918. https://doi.org/10.1113/jphysiol.2009.170662

Sigworth, F.J. 1980. The variance of sodium current fluctuations at the node of Ranvier. *J. Physiol.* 307:97–129. https://doi.org/10.1113/jphysiol.1980.sp013426

Stathopulos, P.B., L. Zheng, G.-Y. Li, M.J. Plevin, and M. Ikura. 2008. Structural and mechanistic insights into STIM1-mediated initiation of store-operated calcium entry. *Cell.* 135:110–122. https://doi.org/10.1016/j.cell.2008.08.006

Stathopulos, P.B., R. Schindl, M. Fahrner, L. Zheng, G.M. Gasmi-Seabrook, M. Muik, C. Romanin, and M. Ikura. 2013. STIM1/Orai1 coiled-coil interplay in the regulation of store-operated calcium entry. *Nat. Commun.* 4:2963. https://doi.org/10.1038/ncomms3963

Tirado-Lee, L., M. Yamashita, and M. Prakriya. 2015. Conformational changes in the Orai1 C-terminus evoked by STIM1 binding. *PLoS One.* 10:e0128622. https://doi.org/10.1371/journal.pone.0128622

Vaeth, M., J. Yang, M. Yamashita, I. Zee, M. Eckstein, C. Knosp, U. Kaufmann, P. Karoly Jani, R.S. Lacruz, V. Flockerzi, et al. 2017. ORAI2 modulates store-operated calcium entry and T cell-mediated immunity. *Nat. Commun.* 8:14714. https://doi.org/10.1038/ncomms14714

Wu, M.M., J. Buchanan, R.M. Luik, and R.S. Lewis. 2006. $Ca^{2+}$ store depletion causes STIM1 to accumulate in ER regions closely associated with the plasma membrane. *J. Cell Biol.* 174:803–813. https://doi.org/10.1083/jcb.200604014

Yamashita, M., P.S. Yeung, C.E. Ing, B.A. McNally, R. Pomès, and M. Prakriya. 2017. STIM1 activates CRAC channels through rotation of the pore helix to open a hydrophobic gate. *Nat. Commun.* 8:14512. https://doi.org/10.1038/ncomms14512

Yang, X., H. Jin, X. Cai, S. Li, and Y. Shen. 2012. Structural and mechanistic insights into the activation of Stromal interaction molecule 1 (STIM1). *Proc. Natl. Acad. Sci. USA.* 109:5657–5662. https://doi.org/10.1073/pnas.1118947109

Yen, M., L.A. Lokteva, and R.S. Lewis. 2016. Functional analysis of Orai1 concatemers supports a hexameric stoichiometry for the CRAC channel. *Biophys. J.* 111:1897–1907. https://doi.org/10.1016/j.bpj.2016.09.020

Yuan, J.P., W. Zeng, M.R. Dorwart, Y.J. Choi, P.F. Worley, and S. Muallem. 2009. SOAR and the polybasic STIM1 domains gate and regulate Orai channels. *Nat. Cell Biol.* 11:337–343. https://doi.org/10.1038/ncb1842

Zal, T., and N.R.J. Gascoigne. 2004. Photobleaching-corrected FRET efficiency imaging of live cells. *Biophys. J.* 86:3923–3939. https://doi.org/10.1529/biophysj.103.022087

Zhang, S.L., Y. Yu, J. Roos, J.A. Kozak, T.J. Deerinck, M.H. Ellisman, K.A. Stauderman, and M.D. Cahalan. 2005. STIM1 is a $Ca^{2+}$ sensor that activates CRAC channels and migrates from the $Ca^{2+}$ store to the plasma membrane. *Nature.* 437:902–905. https://doi.org/10.1038/nature04147

Zhou, Y., P. Srinivasan, S. Razavi, S. Seymour, P. Meraner, A. Gudlur, P.B. Stathopulos, M. Ikura, A. Rao, and P.G. Hogan. 2013. Initial activation of STIM1, the regulator of store-operated calcium entry. *Nat. Struct. Mol. Biol.* 20:973–981. https://doi.org/10.1038/nsmb.2625

Zhou, Y., X. Wang, X. Wang, N.A. Loktionova, X. Cai, R.M. Nwokonko, E. Vrana, Y. Wang, B.S. Rothberg, and D.L. Gill. 2015. STIM1 dimers undergo unimolecular coupling to activate Orai1 channels. *Nat. Commun.* 6:8395. https://doi.org/10.1038/ncomms9395

Zhou, Y., X. Cai, N.A. Loktionova, X. Wang, R.M. Nwokonko, X. Wang, Y. Wang, B.S. Rothberg, M. Trebak, and D.L. Gill. 2016. The STIM1-binding site nexus remotely controls Orai1 channel gating. *Nat. Commun.* 7:13725. https://doi.org/10.1038/ncomms13725

Zhou, Y., R.M. Nwokonko, X. Cai, N.A. Loktionova, R. Abdulqadir, P. Xin, B.A. Niemeyer, Y. Wang, M. Trebak, and D.L. Gill. 2018. Cross-linking of Orai1 channels by STIM proteins. *Proc. Natl. Acad. Sci. USA.* 115:E3398–E3407. https://doi.org/10.1073/pnas.1720810115

Zweifach, A., and R.S. Lewis. 1993. Mitogen-regulated $Ca^{2+}$ current of T lymphocytes is activated by depletion of intracellular $Ca^{2+}$ stores. *Proc. Natl. Acad. Sci. USA.* 90:6295–6299. https://doi.org/10.1073/pnas.90.13.6295